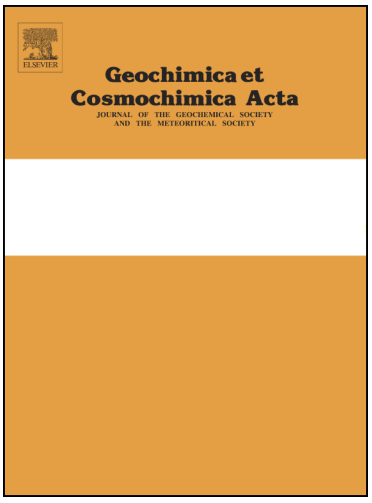

Sequestration of Zn into mixed pyrite-zinc sulfide framboids: A key to Zn cycling in the ocean?

Si-Yu Hu, Katy Evans, Kirsten Rempel, Paul Guagliardo, Matt Kilburn, Dave Craw, Kliti Grice, Jeffrey Dick

PII: S0016-7037(18)30483-6
DOI: https://doi.org/10.1016/j.gca.2018.08.039
Reference: GCA 10912

To appear in: *Geochimica et Cosmochimica Acta*

Received Date: 7 August 2017
Revised Date: 11 June 2018
Accepted Date: 28 August 2018

Please cite this article as: Hu, S-Y., Evans, K., Rempel, K., Guagliardo, P., Kilburn, M., Craw, D., Grice, K., Dick, J., Sequestration of Zn into mixed pyrite-zinc sulfide framboids: A key to Zn cycling in the ocean?, *Geochimica et Cosmochimica Acta* (2018), doi: https://doi.org/10.1016/j.gca.2018.08.039

Sequestration of Zn into mixed pyrite-zinc sulfide framboids: a key to Zn cycling in the ocean?

Si-Yu Hu [a,b,c *], Katy Evans [b], Kirsten Rempel [b], Paul Guagliardo [d], Matt Kilburn [d], Dave Craw [e], Kliti Grice [c], Jeffrey Dick [f]

[a] *CSIRO Mineral Resources, Kensington, WA 6151, Australia*

[b] *School of Earth and Planetary Sciences, Curtin University, GPO Box U1987, Bentley, WA 6845, Australia*

[c] *Western Australia Organic and Isotope Geochemistry Centre, Institute for Geoscience Research, School of Earth and Planetary Sciences, Curtin University, Perth, WA 6845, Australia*

[d] *Centre for Microscopy, Characterisation and Analysis, The University of Western Australia, Crawley, WA 6009, Australia*

[e] *Geology Department, University of Otago, GPO Box 56, Dunedin 9054, New Zealand*

[f] *Key Laboratory of Metallogenic Prediction of Nonferrous Metals and Geological Environment Monitoring, Ministry of Education, School of Geosciences and Info-Physics, Central South University, Changsha 410083, China*

*Corresponding author: siyu.hu@csiro.au

Declarations of interest: none

Abstract

Zinc (Zn) is an important micronutrient in the ocean, and fixation of Zn into organic, trace element-rich sediments is an important contributor to Zn cycling in the ocean. Framboidal sulfides are considered to be the major host for Zn in such settings. The sequestration of Zn into framboids via biotic or abiotic processes is not fully understood, which presents difficulties for interpretation of Zn isotope values in sediments. In this work, we describe a novel type of framboid with mixed pyrite and zinc sulfide (sphalerite or wurtzite) microcrystals from meta-pelites of the Otago Schist, New Zealand. A combination of optical microscopy, scanning electron microscopy (SEM) and nanoscale secondary ion mass spectrometry (NanoSIMS) were utilized to assess the association between Zn, pyrite and organic matter in framboids. The distribution of Zn in framboids is variable. Most pyrite microcrystals include minor amounts of Zn. Trace Zn is also observed to co-locate with organic matter, which occurs on the boundaries of pyrite microcrystals. Finally, Zn is found as single zinc sulfide microcrystals or zinc sulfide rims around pyrite microcrystals within individual framboids. These textures have not been recorded before, to our knowledge. The sequence of events that sequesters Zn into framboids may affect Zn isotope fractionation from seawater to continental margin sediments.

1. Introduction

Framboids are spheroidal aggregates consisting of multiple microcrystals of sulfide minerals and are commonly observed in ancient sedimentary rocks and modern sediments (Love, 1971; MacLean et al., 2008; Gregory et al., 2015; Hu et al., 2016). The formation of framboids has been suggested to be abiotic or biotic (Berner, 1970; Wilkin and Barnes, 1997; MacLean et al., 2008). Laboratory syntheses of pyrite framboids have been extensively conducted, and have shown that framboids can be generated without the involvement of microbial activities, as summarized by Ohfuji and Rickard (2005). However, framboids observed in natural samples are often associated with organic matter (OM_{fr}, defined as the organic matter in framboids), and this OM_{fr} association has been taken to indicate that biotic processes contributed to the formation of framboids (Love, 1957; MacLean et al., 2008; Wacey et al., 2015). Organic matter has been observed to envelop both individual pyrite microcrystals and the complete framboid in modern sediments (MacLean et al., 2008) and ancient sedimentary rock (Wacey et al., 2015), and it has also been demonstrated that the formation of framboids is associated with sulfate-reducing microorganism activities (Machel, 2001; Schoonen, 2004). The degradation of microorganisms or microbial by-products results in the common occurrence of CM_{fr} in the framboidal structure (e.g. Large et al., 2001).

The term "framboids" is usually synonymous with the term "framboidal pyrite" in previous studies because the overwhelming majority of framboids are composed of pyrite microcrystals (e.g. Love, 1971; Berner et al., 2013; Gregory et al., 2015). However, in recent decades, other sulfides, such as cobaltite, chalcopyrite and sphalerite, have also been observed in framboids (Gregory et al., 2015; Hu et al., 2016), suggesting that framboids may also play a role in the cycling of elements other than Fe. Coupled variation of trace elements in framboids, such as Zn, Cu, Pb, Mo, Ni, Cd., have been taken to be indicative of various incorporation processes into the framboidal structure, and to provide valuable information

regarding paleo-ocean environments (Berner et al., 2013; Gregory et al., 2014; Gregory et al., 2017; Large et al., 2017). Amongst those trace elements, Zn has been linked with sulfate-reducing microorganism activities. The precipitation of zinc sulfide (sphalerite or wurtzite) nanoparticle aggregates can be induced by sulfate-reducing bacteria (Labrenz et al., 2000; Moreau et al., 2004; Xu et al., 2016). Sphalerite framboids have been observed in peatlands (Yoon et al., 2012) and at a carbonate-hosted Zn-Pb deposit (Kucha et al., 2010). Co-location of sphalerite patches around 10 μm in size with OM_{fr} in pyrite-dominated polyframboids was interpreted as a record of the incorporation of Zn into framboids via sulfate-reducing bacterial activities (Hu et al., 2016), providing new explanations for the presence of zinc sulfide micro-inclusions in pyrite-rich framboids (Gregory et al., 2015). However, it has also been suggested that Zn substitutes into the pyrite structure via solid solution or precipitates as micro-inclusions without the involvement of microbial activity (Algeo and Maynard, 2004; Berner et al., 2013). Further examination of Zn occurrences in framboids, including the distribution of trace Zn, and the estimation of relevant biotic and abiotic contribution to the framboid formation, is essential to better understand the Zn sequestration processes. Such an understanding is vital if Zn is to be applied as a paleo-environment proxy (e.g. Tribovillard et al., 2006).

In addition, Zn is a widespread trace element and an essential micronutrient in the ocean (John and Conway, 2014; Conway and John, 2015). Recent studies have demonstrated that seawater preferentially concentrates heavy $\delta^{66}Zn$, while organic, trace element-rich continental margin sediments are sinks for light $\delta^{66}Zn$ (Conway and John, 2014; Little et al., 2014; Zhao et al., 2014; Little et al., 2016). Observations suggest that Zn isotope fractionation occurs during Zn fixation in those settings, the process of which is still controversial. Framboids are common in such sediments and are thought to be the major host for Zn and other trace elements in sediments (Large et al., 2014; Gregory et al., 2015; Hu et

al., 2016). Hence, an understanding of the pathway via which Zn is assimilated into framboids is also necessary to provide insights for Zn isotope fractionation during sediment deposition.

A wide variety of techniques have been previously applied to characterize framboids, such as scanning electron microscopy coupled with energy-dispersive X-ray spectroscopy (SEM-EDS), electron microprobe analysis (EPMA) and laser ablation inductively coupled plasma mass spectrometry (LA-ICP-MS) (Lowers et al., 2007; MacLean et al., 2008; Gregory et al., 2015). Additionally, sulfur isotopes analysed with secondary ion mass spectrometry (SIMS) can help to confirm the source of sulfur in sulfides and the isotopes of sulfides of various morphologies has the potential to be linked to the formation pathways (Gomes et al. 2018). However, due to the small size (~ 1 μm) of individual microcrystals and different degrees of mixing of various types of microcrystals within framboids, these conventional techniques lack the spatial resolution necessary to provide detailed information on the micron scale crystal types described here. The analysis of sulfur isotopes in sphalerite is also challenging due to the orientation effects caused by the difference between crystal orientation of grains and the incident primary beam (Kozdon et al, 2010). Nanoscale secondary ion mass spectrometry (NanoSIMS) can determine the distribution of trace elements *in situ* with submicron resolution relatively quickly (Kilburn and Clode, 2013; Wacey et al., 2015). Additionally, NanoSIMS is able to map the distribution of nitrogen (N) and carbon (C), which are key elements involved in biological processes (Kilburn and Wacey, 2011) and present as trace in framboids from ancient sedimentary rocks. The low atomic number of N and C presents difficulties for conventional EDS or wavelength-dispersive X-ray spectroscopy (WDS) analysis (Wacey et al., 2015), but their distribution is a valuable indication of the location of OM_{fr} that occurs as a precursor to framboids, and thus provides significant information on the role of bacteria in framboid growth.

In this study, we describe a novel type of pyrite-zinc sulfide mixed framboids composed of multiple equidimensional pyrite and zinc sulfide microcrystals from low metamorphic grade metasedimentary rock (prehnite-pumpellyite facies) of Otago Schist, New Zealand. A combination of optical microscopy, SEM and NanoSIMS was performed to characterize the framboids and determine the element distribution within framboids. The distribution of metals (ZnS, FeS) and OM_{fr} (C, N) are compared to determine the spatial relationships between Zn, pyrite and OM_{fr}, and constrain the processes via which Zn is incorporated into framboids.

2. Geological Background and sampling

The Otago Schist is a Paleozoic to Mesozoic turbidite sequence comprising quartzo-feldspathic psammite and pelites, deposited in a continental margin setting (MacKinnon, 1983; Craw, 2002). These schists were metamorphosed during the collision of the Caples and Torlesse Terranes (Mortimer, 2000), and uplifted to form a symmetrical metamorphosed belt. The belt comprises a core zone of upper greenschist facies rocks flanked on either side by zones of progressively lower grade rocks (Fig. 1) (Mortimer, 1993; Mortimer, 2000). The metamorphic grade increases from prehnite-pumpellyite (P-P) facies on the margins, moving through pumpellyite-actinolite (P-A) facies to upper greenschist (G-S) facies within the core zone of the schist belt (Fig. 1). The rocks become progressively more recrystallized and foliated through this increase in metamorphic grade, and the schists in the core of the belt have been pervasively recrystallized with several generations of folding and foliation development (Mortimer, 1993). The P-P facies is dominated by meta-pelite and the primary minerals include pyrite-dominated framboids, quartz, albite, muscovite, chlorite, epidote, stilpnomelane, pumpellyite and prehnite. Framboids are a major host for trace elements in these rocks and have been suggested to be the source for Au and other trace metals in

orogenic gold deposits in the Otago Schist (Pitcairn et al., 2006; Large et al., 2012; Hu et al., 2016).

The sample (FF-16) from P-P facies rocks at Fiddlers Flat is a metapelite and was analysed after selection from around 40 samples collected in the field (Fig. 1). Details of the sampling locations have been described by Hu et al. (2015), and organic matter associations and their variation with metamorphic grade have been described in Hu et al. (2015) and Henne and Craw (2012).

3. Methods

An aliquot of the sample was crushed into powder for bulk zinc concentration analysis in a tungsten carbide ring mill. Analyses were conducted by Intertek Genalysis Lab (Perth, Australia). Zinc content was obtained by preparing a fused disc of the sample, which was analysed by X-ray fluorescence (XRF) spectrometry. A second aliquot was cut from fresh rock sample, embedded in a one-inch resin mount and polished. Mineral assemblages were characterized by optical microscopy and framboids were further characterized with SEM-EDS at the Department of Applied Geology, Curtin University (Perth, Australia) and Commonwealth Science and Industry Research Organisation (CSIRO) Mineral Resources (Perth, Australia). Ten polyframboids were examined with optical microscopy and SEM and key areas from three polyframboids were chosen for further NanoSIMS mapping. The chosen polyframboids comprise aggregates of individual microcrystals with few secondary sulfides, such as chalcopyrite and cobaltite, and are morphologically different to the polyframboids described and analysed by Hu et al. (2016).

NanoSIMS analysis was performed with a Cameca NanoSIMS 50 at the Centre for Microscopy, Characterization and Analysis (CMCA), at University of Western Australia. The mounts were coated with silver at high voltage for conductivity. Measurements were

performed with a Cs^+ primary beam, with a spot size of approximately 100 nm, an impact energy of 16 keV, and a beam current of approximately 2 pA. The instrument was operated in multicollector mode with simultaneous detection of $^{12}C_2^-$, $^{12}C^{14}N^-$, $^{56}Fe^{32}S^+$ and $^{65}Zn^{32}S^+$ from the same analysis region. It is noted that C in $^{12}C_2^-$ is the same as C in $^{12}C^{14}N^-$. Prior to imaging, a 500 pA primary Cs^+ current of > 2 x 10^{17} ions/cm^2 was used to presputter in order to remove surface contamination and implant Cs^+ ions to reach a steady-state of ion emission. Secondary ion images were obtained by rastering the primary ion beam with areas of 8 x 8 – 45 x 45 μm^2, resolution of 256 x 256 pixels and dwell times of 45–250 ms per pixel. Note that Zn and Fe are measured as $^{65}Zn^{32}S$ and $^{56}Fe^{32}S$ respectively by NanoSIMS, so Zn and Fe mentioned in the following text refers to Zn and Fe bound to S.

The data were processed with OpenMIMS software developed by the National Resource for Imaging Mass Spectrometry, Harvard University. Counts of elements are positively correlated to the element concentrations. Counts of each element from each grain were extracted and normalized to their respective secondary electron (SE) counts to remove artefacts caused by topography.

4. Results

4.1 Geochemical analysis and petrographic observations

The bulk Zn content of this sample is 130 ppm, an intermediate between average Zn concentration in shale (90 ppm) and pelagic clay (170 ppm) (Li and Schoonmaker, 2013).

The term polyframboids here is used to describe composites of framboids and microcrystals. Polyframboids are common in FF-16, and occur together with quartz and clay minerals, such as muscovite and stilpnomelane; the sheet silicate minerals, especially stilpnomelane, show a preferred orientation and, are slightly aligned with the bedding and framboids are observed to be wrapped by the clay minerals (Fig. 2 & 3). The polyframboids

are generally rounded, elliptical or irregular in shape, with size of up to 200 x 50 µm (Fig. 2). The size of single framboids ranges from ~10 to 30 µm in diameter. Mineralogically, the composition ranges from pyrite-dominated to a mix of pyrite (60%)-zinc sulfide (40%) (Fig. 2). Pyrite and zinc sulfide microcrystals are equidimensional (Fig. 3). The microcrystals are distributed in an ordered fashion in some framboids, with hexagonal or pseudohexagonal symmetry (Fig. 3a), or, in other cases, present as apparently randomly distributed aggregates of crystals. Small framboids of less than 10 µm were most commonly well-organized with hexagonal symmetry (Fig. 3b). Single microcrystals within the framboids vary from euhedral cubic or octahedral to sub-rounded (Fig. 3b). The compositions of microcrystals, analysed with semi-quantitative EDS analysis, range from variably zinc-rich pyrite, or zinc sulfide with minor Fe. Given the small size of the crystals, it was not possible to distinguish between wurtzite and sphalerite, so the term zinc sulfide is used to cover both.

4.2 NanoSIMS Observations

4.2.1 Fe and Zn mapping

Four types of microcrystals with differing Fe and Zn concentrations were recognized within the framboids.

Type 1: Pyrite microcrystals with homogeneous trace Zn

Pyrite, characterized by high counts of Fe (as $^{56}Fe^{32}S$) and trace Zn (as $^{65}Zn^{32}S$), is the dominant microcrystal type in pyrite-rich framboids (Fig. 4a). The distribution of trace Zn is homogeneous within grains. Individual microcrystals are sub-rounded with sizes of 1–2 µm. On an element profile across a microcrystal (from x to x'), Fe and Zn contents show similar trends (Fig. 4a). Normalized Zn counts were plotted against those for Fe, and display a positive correlation in these microcrystals.

Type 2: Pyrite microcrystals with trace Zn concentrated on boundaries

Type 2 microcrystals are also characterized by high Fe and low Zn contents, and occur in pyrite-dominated framboids, but show octahedral morphology. In contrast to the homogeneous trace Zn distribution observed in the type 1 microcrystals, trace Zn has higher concentrations at the boundaries than inside the grain (Fig. 4b). On an element profile across a type 2 microcrystal (from x to x'), Zn counts are consistently low in the centre of the grain, and higher on the boundary where Fe counts are relatively low (Fig. 4b); however, Zn concentrations are not sufficiently high to interpret the Zn-rich region on the boundaries as zinc sulfide crystals.

Type 3: Microcrystals with intergrown pyrite and zinc sulfide

Type 3 microcrystals are observed in pyrite-zinc sulfide mixed framboids (Fig. 5a). Plots of SE-normalized Zn against Fe reveal well-delineated groups of data with both high and low Zn/Fe ratios, which correspond to zinc sulfide and pyrite respectively (Fig. 5c). The microcrystals are rare and display an octahedral morphology with cores of pyrite and rims of zinc sulfide (Fig. 5b). The diameter of an entire type 3 microcrystal is around 1 μm, whereas that of the inner pyrite core varies from 0.06 to 0.6 μm.

Type 4: Zinc sulfide microcrystals

Zinc sulfide also occurs as individual crystals distinguished by high Zn counts. The zinc sulfide microcrystals are otherwise similar to adjacent pyrite microcrystals (Fig. 5b) in that the two minerals have similar crystal shape and size (around 1 μm). There is no discernible pattern to the distribution of pyrite and zinc sulfide, so they are taken to be randomly distributed.

4.2.2 Distribution of OM_{fr}

OM_{fr}-pyrite relationships

Carbon-nitrogen (CN, as $^{12}C^{14}N$) mapping reveals that CN is concentrated on the boundaries of pyrite microcrystals, in an annular zone (Fig. 6a). The CN index, defined as the ratio of counts of CN/ (CN+Fe+Zn), is used to represent, semi-quantitatively, the concentration of CN relative to that of other elements. A line profile through a type 2 microcrystal shows high Fe with low Zn, CN and carbon (C_2, as $^{12}C_2^-$) contents within the crystal. The concentrations of CN are higher on both boundaries than inside the grain, and the boundaries are associated with a high CN index. C_2 follows a similar trend to CN, but the correlation between the two parameters is weak. Counts of Zn are generally low in the C- and CN-rich areas, but Zn counts are highest at one of the grain boundaries, co-located with a peak in CN concentration.

OM_{fr} -zinc sulfide relationships

Zinc sulfide (type 4 microcrystal) is characterized by high Zn and CN contents with minor Fe and C_2 (Fig. 6b). On a profile across a type 4 microcrystal, Zn, Fe and CN have similar trends with wide, superimposed peaks (Fig. 6b). The concentration of Zn is high relative to that of Fe, but there is almost no Zn or Fe in the middle of the grain, in an area interpreted as a hole in the grain. The concentration of CN is relatively high across the grain, and the CN index is highest at the hole. The contents of Zn, Fe and CN are low on one side of the "hole" and high on the other side. Carbon counts are generally low with a small peak on the boundary.

5. Discussion

5.1 Zn and pyrite relationships

The abundance of Zn in the framboids is highly variable with four distinct types of microcrystals. Trace zinc is distributed homogeneously in pyrite microcrystal as type 1 (Fig. 4a), or concentrated at the boundaries of pyrite grains as type 2 (Fig. 4b). In types 3 and 4, pyrite microcrystals are intergrown with or co-exist with zinc sulfide microcrystals, respectively, within a single framboid (Fig. 5). The relative proportions of four types of microcrystals vary from different framboids with type 1 (60-70%) > type 4 (26-36%) > type 3 (3%) > type 2 (1%). Type 2 and type 3 microcrystals are uncommon. Inclusion of zinc sulfide in pyrite framboids has been recorded by other researchers (e.g. Berner et al., 2013; Gregory et al., 2015). However, descriptions of the type 2, 3 and 4 microcrystals are, to the best of our knowledge, presented here for the first time. It is interesting to consider how Zn incorporation into sulfide, with or without a role of co-existing OM_{fr}, was able to produce the complex variation in various microcrystals. Further, if there are multiple routes for Zn incorporation then there may be implications for the interpretation of Zn isotope data from sedimentary rocks. These issues are discussed further below.

5.2 OM_{fr} and sulfide associations

C_2 and CN have similar distributions in profiles through pyrite and zinc sulfide microcrystals, but CN tends to have higher count rates than C_2 (Fig. 6). CN, represented by $^{12}C^{14}N$, indicates the co-occurrence of C and N. The two elements are important components of organic matter, which are produced via microbial activities (Braissant et al., 2007) and have been widely used as parameters for biosignatures in ancient rocks (e.g. Wacey et al., 2015 and Kilburn and Wacey, 2011).

In this study, given that CN has higher count rates and therefore higher signal:noise than C_2, CN was considered to represent OM_{fr}, consistent with the strategy employed by other workers (Wacey et al., 2010; Wacey et al., 2015). The location of CN, concentrated on the

boundaries of pyrite (Fig. 6a), is consistent with the observations in MacLean et al. (2008) and Wacey et al. (2015), who both recorded single pyrite microcrystals enclosed by OM_{fr}, and proposed that pyrite grows within biofilms or an organic matrix as the result of bacterial activities. Zinc, concentrated at the boundaries of pyrite in type 2 microcrystal, co-locates with CN in some cases (Fig. 6a & b). This indicates that ZnS may be deposited *in situ* with the OM_{fr} matrix, as discussed further below.

5.3 Sequestration of Zn into sulfide in framboids

Most pyrite framboids found in natural samples are thought to be a consequence of sulfate reducing bacteria (SRB) activity, during which SRB use organic matter as an electron source to produce hydrogen sulfide, with which Fe^{2+} complexes to form mackinawite, and further transforms to greigite and pyrite (Donald and Southam, 1999; Machel, 2001; Schoonen, 2004; Picard et al., 2018). In addition to the OM evidence in this study, it is noted that the size and morphology of microcrystals in the studied framboids are similar to those biogenic sulfides observed in previous studies (e.g. MacLean et al., 2007; MacLean et al., 2008). Although the contribution of microorganism to the nucleation and morphology evolution of sulfides during the formation of framboids are still unknown (Picard et al., 2016), parameters such as size and morphology can be used as evidence for a biotic origin for framboids. This proposal is supported by a recent study which indicates that sulfate-reducing bacteria have significant impacts on the size and aggregation of mackinawite and greigite crystals in comparison with sulfides precipitated under abiotic conditions (Picard et al., 2018).

Zn hosted by pyrite framboids has been suggested to occur as solid solution in pyrite, with Zn substituting for Fe, or as zinc sulfide inclusions (Morse and Luther, 1999; Algeo and Maynard, 2004; Berner et al., 2013; Gregory et al., 2015). In Zn-rich environments, sphalerite is deposited as framboids within SRB-rich biofilms without the presence of other sulfides

(Labrenz et al., 2000; Bawden et al., 2003; Labrenz and Banfield, 2004). Alternatives to Zn immobilization by SRB activity are precipitation of zinc sulfide directly from seawater without organic mediation, complexation of Zn with organic matter, such as humic acid (Jouvin et al., 2009) or sorption onto bacterial cell surfaces directly when Zn interacts with microorganisms (Eide, 2006; Kafantaris and Borrok, 2014), without any necessity for SRB. Unfortunately, due to technical limitations related to the primary beam used for NanoSIMS analysis, Zn without sulfur could not be measured, so the distribution of Zn co-located with OM_{fr} without sulphur, is unknown. It has also been suggested that Zn occurs within the clay-organic matter matrix, or in both pyrite and matrix in marine sedimentary rocks, with the distribution controlled by redox state and sulfur budgets during diagenesis (Large et al., 2017). The Zn budget in the sample investigated in this study was documented by Hu et al. (2016), who showed that framboids host 90% of Zn. Turbiditic sedimentary rock such as those from which FF-16 are taken are common in the geological record. However, clay and organic matter in the matrix may play a more important role as the host for Zn in rocks from other settings.

The co-location of zinc sulfide and OM_{fr} observed in zinc sulfide framboids (Labrenz et al., 2000; Moreau et al., 2004), and negative sulfur isotopes of sphalerite in such structures (Bawden et al., 2003) are consistent with the formation of zinc sulfide framboids via SRB activity with some involvement of OM_{fr}. A previous study of a biofilm sample from an anaerobic environment revealed that zinc sulfide nanoparticles coat the surface of bacterial filaments while euhedral pyrite and pyrite framboids precipitate within the biofilm rather than nucleating on bacterial surfaces (MacLean et al., 2007). This spatial relationship indicates that zinc sulfide is likely to have more affinity to OM_{fr} than pyrite and that it is deposited prior to pyrite in Zn-rich environment, consistent with previous results indicating that Zn^{2+} in seawater has faster water exchange reaction kinetics than Fe^{2+}, causing zinc sulfide to be

deposited prior to iron sulfide (Morse and Luther, 1999). Therefore, the co-location of ZnS (both as trace amounts and zinc sulfide) and OM_{fr} observed in framboids of this study is consistent with SRB activity. The observed textures also suggest that OM_{fr} may act as an intermediary that concentrates ZnS, while Fe is precipitated as iron sulfide microcrystals within the OM matrix of the framboid.

Metastable but kinetically favoured mackinawite often transforms to pyrite after precipitation (Donald and Southam, 1999). Similarly, sphalerite and wurtzite are precipitated together during SRB activity (Moreau et al., 2004; MacLean et al., 2007), but the polymorph present does not need to be specified to characterise the pathway of Zn incorporated into framboids.

Conceptual Model

It has been suggested that the formation of pyrite in sediments is controlled by the supply of organic matter (defined as OM_{influx}), dissolved sulfate concentration and the availability of reactive Fe-rich minerals (Berner, 1970; Berner, 1984; Zhou et al., 2014). Redox and pH also play a role in sulfide stability (Rickard, 1970; Zhou et al., 2014). The rate of SRB activity is dominated by OM_{influx} and sulfate supply (Rickard, 2012). The four types of microcrystals observed in this study could therefore form in an evolving system subject to a complex interdependent variation of these parameters.

The conceptual model presented below is speculative, but forms the basis for hypotheses and further focussed study of the behaviour of Zn in framboids forming anoxic-sulfidic conditions. The model, illustrated in Fig. 7, begins with organic matter-rich sediments in a euxinic environment. Pores within the sediments below the redox interface contain an aqueous solution that had the composition of seawater when first trapped. Metals are sourced both from seawater and desorption from dead marine plankton in the organic component of

the sediment (Brumsack, 2006). Redox, pH, sulfate and metal concentrations within the pore-water evolve continuously as diagenesis and framboid formation proceeds. The system is envisaged as being almost closed, although some influx of externally derived fluids, such as fresh seawater, could occur. In such environments, OM_{influx} and sulfate are initially abundant and SRB activity rate is not limited by the supply of the reactants. Under these circumstances, the Zn:Fe ratio is the dominant parameter that determines the extent of Zn incorporation into framboids. When Zn:Fe is high in the porewater, zinc sulfide deposits directly on the bacterial cell wall during bacterial activity, aided by rapid kinetics of ZnS formation, to form type 4 zinc sulfide (Fig. 7). The bacterial cell degrades into OM_{fr} later. Precipitation of zinc sulfide decreases the Zn:Fe ratio in the pore-water. When Zn in solution decreases to the point that zinc sulfide formation ceases or slows significantly, Zn may be deposited on OM_{fr} directly, while pyrite or mackinawite is precipitated within the OM_{fr} framework as type 2 microcrystals. Precipitation of iron sulfides would increase the Zn:Fe ratio in the porewater to the point that ZnS precipitation rates could increase, so that ZnS formation after pyrite or mackinawite precipitation had begun could result in the formation of type 3 microcrystals where pyrite is enclosed by ZnS to form a single microcrystal.

Fluctuation in other parameters, such as sulfate concentration, redox state and pH could drive switches from ZnS precipitation to Zn sorption on OM and back again, since otherwise porewater solutions would simply reach equilibrium with ZnS. Pyrite or mackinawite precipitation at this point would include low concentrations of Zn via adsorption on the growth surfaces of pyrite or its precursor. This process would form the type 1 microcrystals (Morse and Arakaki, 1993).

It is also interesting to speculate if precipitation of the different microcrystal types is cyclical, or whether the sequence is progressive. It seems likely that Zn:Fe ratios fluctuate in response to sulfide precipitation, the sorption and deposition of metals from the OM_{influx}, and

interactions with fluids external to the porewater system. Further, the supply of hydrogen sulfide would also vary in response to changing activity of SRB. It is therefore possible that there could be repeated cycles of formation of the different types of microcrystal, and that the different types could form simultaneously in different parts of the framboids if equilibrium or diffusion lengthscales were sufficiently short. However, it should be noted that, while pyrite surrounded by zinc sulfide is common, the reverse is not seen. This observation could be taken as support for a unidirectional evolution of the system with time. An alternative explanation is that there may be features of the surface chemistry of pyrite or its precursor mackinawite that facilitated ZnS precipitation on Fe-sulfide, while the reverse may not have been true for ZnS. Alternatively, differences in the capacity of the precursor and final phases to form Zn-Fe solid solutions may play a role in the observed textures, but these are not well known and thus lie beyond the scope of this discussion. Further research is needed to distinguish between these possibilities.

Effects of metamorphism

This sample has been metamorphosed to prehnite-pumpellyite facies so metamorphic modification of the textures post diagenesis must be accounted for in their interpretation. The presence of CN, rather than C alone, implies that the organic matrix is preserved (Fig. 6b), to some extent, at prehnite-pumpellyite facies. Further, the morphology of the framboids is identical to those in unmetamorphosed rocks (Ohfuji et al., 2005) and modern sediments (Wilkin et al., 1996). Framboid morphology changes readily with any recrystallization or compositional modifications (Sawlowicz, 1993; Large et al., 2009), so the absence of any evidence for such modification, and the textural relationship between the framboids and foliated sheet silicates in Fig. 2 & 3 are taken as evidence for a lack of metamorphic and hydrothermal alteration.

Comparison with previous study in Hu et al. (2016)

Hu et al. (2016) noted some of the features recorded here, such as the co-location of zinc sulfide and OM_{fr}, in rocks from the same location. In that work, a combination of SEM, Raman spectroscopy, synchrotron X-ray fluorescence microscopy and LA-ICP-MS was performed to characterize the polyframboids. Type 2, 3 and 4 microcrystals were not observed in that study, and the Zn concentrations in type 1 microcrystals were not described, because the spatial resolution and detection limit of the techniques used by Hu et al. (2016) were not sufficient to reveal the different types of microcrystal. The combined results from this study and that of Hu et al. (2016) suggest that co-location of zinc sulfide and OM makes a significant contribution to the Zn-sequestration process, but that multiple additional processes must also be considered if Zn sequestration is to be better understood.

5.4 Implications for Zn isotope fractionation in continental margin sediments

Recent studies show that organic trace element-rich continental margin sediments are sinks for light δ^{66}Zn (as low as ~ -0.40 ‰), in contrast to heavy δ^{66}Zn in seawater (~ +0.53 ‰) and other outputs (such as oxic sediments, δ^{66}Zn ~ +1.0 ‰) (Little et al., 2014; Zhao et al., 2014; Little et al., 2016). Different fractionation factors are likely to pertain to fractionation of Zn between seawater and zinc sulfide, and between OM and zinc sulfide, so the proposed diversity of pathways for sequestration of Zn from seawater into framboids has implications for Zn isotope fractionation during the deposition of continental margin sediments. As framboids are the major host for Zn in rocks of the type studied here, sequestration of Zn from modified seawater in pores into framboids is the overall control on Zn isotope fractionation processes during sedimentation.

The observations presented in this study suggest that fixation of Zn in framboids is the result of a combination of three processes: (1) zinc sulfide precipitation during BSR activity

(type 2, 3, 4); (2) assimilation of Zn absorbed onto OM_{fr} (ZnS-OM_{fr} association); and (3) direct incorporation into pyrite (type 1). All of these processes will be associated with fractionation of Zn isotopes. For example, ZnS precipitated under microbially-mediated sulfate reducing conditions sequesters the lighter Zn isotope ($\Delta_{ZnS\text{-}solution}{}^{66}Zn \sim -0.27‰$) (Jamieson-Hanes et al., 2017). For process 2, the complexation with humic acid is associated with a fractionation factor of ~ +0.24‰ for $\Delta_{humic\ acid\text{-}free\ ions}{}^{66}Zn$ (Jouvin et al., 2009). Bacterial surface adsorption and intracellular incorporation has been noted to result in Zn isotope fractionation in a wide range ($\Delta_{adsorbed\text{-}solution}{}^{66}Zn \sim -0.2‰$ to +0.5‰), depending on Zn:bacteria ratio and bacterial species (Kafantaris and Borrok, 2014). Zn isotopes are therefore likely to be fractionated during incorporation into OM_{fr} during SRB activity, but this fractionation is likely to be a complex function of multiple factors, such as metal-organic binding efficiency and bacterial and metal speciation. The incorporation of Zn into pyrite (process 3) may induce isotope fractionation as well, but, again, little is known of the magnitude of this fractionation. *In situ* measurements of Zn isotope ratios in co-existing sulfides and OM_{fr} were beyond the scope of this study, but are strongly recommended as a basis for a better understanding of diagenetic effects on Zn isotope fraction.

6. Conclusions

The abundance of Zn is highly variable in framboids. NanoSIMS analysis revealed four types of microcrystals hosted by polyframboids in a sulphur-rich pelitic sample from the Otago Schist, including three types not previously described. Textures indicate that the Zn sequestration process is dominated by biotic processes coupled with minor abiotic processes. Pyrite microcrystals are characterized by high Fe concentrations and minor, homogeneously distributed, trace concentrations of Zn. Co-location of ZnS and OM_{fr} occurs on the boundaries of pyrite microcrystals in some cases. Zn also occurs as zinc sulfide microcrystals

within pyrite-dominated polyframboids; the zinc sulfide microcrystals have a similar crystal shape and size to the pyrite microcrystals, or occur as zinc sulfide rims around pyrite cores within single framboids. The different types of microcrystal in the framboids may be a record of cyclical variations in the mechanism of Zn incorporation into framboids as a consequence of sulfate reducing bacteria activity associated with evolving Zn/Fe ratios in a closed, or nearly closed, pore-water system. The variation in Zn incorporation pathway may help to explain observed variability in Zn isotope fractionation between seawater and continental margin sediments. However, better constraints on the extent of Zn isotope fractionation, and the conditions under which Zn combines with OM and sulfides, are required to quantify the extent to which changes in sequestration pathway affect the fractionation of Zn isotopes during sequestration into sediments.

Acknowledgements

All the authors acknowledge the support from the CSIRO Mineral Resources Flagship Cluster for Organic Geochemistry of Mineral Systems led by Curtin University and additional support from the WA-Organic and Isotope Geochemistry Centre (WA-OIGC), The Institute of Geoscience Research (TIGeR) and Curtin University. S.H. acknowledges the receipt of Chinese Scholarship Council (CSC)-Curtin International Postgraduate Research Scholarship (CIPRS), CSIRO PhD Top-up Scholarship. Additional funding support was provided by the Ministry of Business, Innovation and Employment, New Zealand. Associate Editor Sabine Kasten and three anonymous reviewers are thanked for editorial handling and perceptive reviews that improved the manuscript.

References

Algeo T. J. and Maynard J. B. (2004) Trace-element behavior and redox facies in core shales

of Upper Pennsylvanian Kansas-type cyclothems. *Chem. Geol.* **206**, 289–318.

Bawden T. M., Einaudi M. T., Bostick B. C., Meibom A., Wooden J., Norby J. W., Orobona M. J. T. and Chamberlain C. P. (2003) Extreme 34S depletions in ZnS at the Mike gold deposit, Carlin Trend, Nevada: Evidence for bacteriogenic supergene sphalerite. *Geology* **31**, 913–916.

Berner R. (1970) Sedimentary pyrite formation. *Am. J. Sci.* **268**, 1–23.

Berner R. A. (1984) Sedimentary pyrite formation: An update. *Geochim. Cosmochim. Acta* **48**, 605–615.

Berner Z. A., Puchelt H., Nöltner T. and Kramar U. (2013) Pyrite geochemistry in the Toarcian Posidonia Shale of south-west Germany: Evidence for contrasting trace-element patterns of diagenetic and syngenetic pyrites. *Sedimentology* **60**, 548–573.

Braissant O., Decho A. W., Dupraz C., Glunk C., Przekop K. M. and Visscher P. T. (2007) Exopolymeric substances of sulfate-reducing bacteria: Interactions with calcium at alkaline pH and implication for formation of carbonate minerals. *Geobiology* **5**, 401–411.

Brumsack H. J. (2006) The trace metal content of recent organic carbon-rich sediments: Implications for Cretaceous black shale formation. *Palaeogeogr. Palaeoclimatol. Palaeoecol.* **232**, 344–361.

Conway T. M. and John S. G. (2014) Global Biogeochemical Cycles isotopes in the North Atlantic Ocean. *Glob. Biogeochem. Cycles Res.*, 1111–1128.

Conway T. M. and John S. G. (2015) The cycling of iron, zinc and cadmium in the North East Pacific Ocean - Insights from stable isotopes. *Geochim. Cosmochim. Acta* **164**, 262–283. Available at: http://dx.doi.org/10.1016/j.gca.2015.05.023.

Craw D. (2002) Geochemistry of late metamorphic hydrothermal alteration and graphitisation of host rock, Macraes gold mine, Otago Schist, New Zealand. *Chem. Geol.* **191**, 257–275.

Donald R. and Southam G. (1999) Low temperature anaerobic bacterial diagenesis of ferrous monosulfide to pyrite. *Geochim. Cosmochim. Acta* **63**, 2019–2023.

Eide D. J. (2006) Zinc transporters and the cellular trafficking of zinc. *Biochim. Biophys. Acta - Mol. Cell Res.* **1763**, 711–722.

Gomes M. L., Fike D. A., Bergmann K. D., Jones C. and Knoll A. H. (2018) Environmental insights from high-resolution (SIMS) sulfur isotope analyses of sulfides in Proterozoic microbialites with diverse mat textures. *Geobiology* **16**, 17–34.

Gregory D. D., Large R. R., Halpin J. A., Baturina E. L., Lyons T. W., Wu S., Danyushevsky L., Sack P. J., Chappaz A., Maslennikov V. V and Bull S. W. (2015) Trace Element Content of Sedimentary Pyrite in Black Shales. *Econ. Geol.* **110**, 1389–1410.

Gregory D. D., Lyons T. W., Large R. R., Jiang G., Stepanov A. S., Diamond C. W., Figueroa M. C. and Olin P. (2017) Whole rock and discrete pyrite geochemistry as complementary tracers of ancient ocean chemistry: An example from the Neoproterozoic Doushantuo Formation, China. *Geochim. Cosmochim. Acta* **216**, 201–220.

Gregory D., Meffre S. and Large R. (2014) Comparison of metal enrichment in pyrite framboids from a metal-enriched and metal-poor Estuary. *Am. Mineral.* **99**, 633–644.

Henne A. and Craw D. (2012) Synmetamorphic carbon mobility and graphite enrichment in metaturbidites as a precursor to orogenic gold mineralisation, Otago Schist, New Zealand. *Miner. Depos.* **47**, 781–797.

Hu S., Evans K., Craw D., Rempel K., Bourdet J., Dick J. and Grice K. (2015) Raman characterization of carbonaceous material in the Macraes orogenic gold deposit and metasedimentary host rocks, New Zealand. *Ore Geol. Rev.* **70**, 80–95.

Hu S. Y., Evans K., Fisher L., Rempel K., Craw D., Evans N. J., Cumberland S., Robert A. and Grice K. (2016) Associations between sulfides, carbonaceous material, gold and

other trace elements in polyframboids: Implications for the source of orogenic gold deposits, Otago Schist, New Zealand. *Geochim. Cosmochim. Acta* **180**, 197–213.

Jamieson-Hanes J. H., Shrimpton H. K., Veeramani H., Ptacek C. J., Lanzirotti A., Newville M. and Blowes D. W. (2017) Evaluating zinc isotope fractionation under sulfate reducing conditions using a flow-through cell and in situ XAS analysis. *Geochim. Cosmochim. Acta* **203**, 1–14.

John S. G. and Conway T. M. (2014) A role for scavenging in the marine biogeochemical cycling of zinc and zinc isotopes. *Earth Planet. Sci. Lett.* **394**, 159–167.

Jouvin D., Louvat P., Juillot F. and Maréchal C. (2009) Zinc isotopic fractionation: why organic matters. *Environ. Sci. Technol.* **43**, 5747–5754.

Kafantaris F. C. A. and Borrok D. M. (2014) Zinc isotope fractionation during surface adsorption and intracellular incorporation by bacteria. *Chem. Geol.* **366**, 42–51.

Kilburn M. R. and Clode P. L. (2013) Elemental and Isotopic Imaging of Biological Samples Using NanoSIMS BT - Electron Microscopy. In *Electron Microscopy* pp. 733–755.

Kilburn M. R. and Wacey D. (2011) Elemental and Isotopic Analysis By Nanosims: Insights for the Study of Stromatolites and Early Life on Earth. In *Stromatolites: Interaction of Microbes with Sediments* pp. 465–493.

Kozdon R., Kita N. T., Huberty J. M., Fournelle J. H., Johnson C. A. and Valley J. W. (2010) In situ sulfur isotope analysis of sulfide minerals by SIMS: Precision and accuracy, with application to thermometry of ~3.5Ga Pilbara cherts. *Chem. Geol.* **275**, 243–253.

Kucha H., Schroll E., Raith J. G. and Halas S. (2010) Microbial sphalerite formation in carbonate-hosted Zn-Pb ores, Bleiberg, Austria: Micro- to nanotextural and sulfur isotope evidence. *Econ. Geol.* **105**, 1005–1023.

Labrenz M. and Banfield J. F. (2004) Sulfate-reducing bacteria-dominated biofilms that precipitate ZnS in a subsurface circumneutral-pH mine drainage system. *Microb Ecol* **47**,

205–217.

Labrenz M., Druschel G. K., Thomsen-Ebert T., Gilbert B., Welch S. a, Kemner K. M., Logan G. a, Summons R. E., De Stasio G., Bond P. L., Lai B., Kelly S. D. and Banfield J. F. (2000) Formation of sphalerite (ZnS) deposits in natural biofilms of sulfate-reducing bacteria. *Science* **290**, 1744–1747.

Large D. J., Fortey N. J., Milodowski A. E., Christy A. G. and Dodd J. (2001) Petrographic observations of iron, copper, and zinc sulfides in freshwater canal sediment. *J. Sediment. Res.* **71**, 61–69.

Large R. R., Danyushevsky L., Hollit C., Maslennikov V., Meffre S., Gilbert S., Bull S., Scott R., Emsbo P., Thomas H., Singh B. and Foster J. (2009) Gold and trace element zonation in pyrite using a laser imaging technique: Implications for the timing of gold in orogenic and carlin-style sediment-hosted deposits. *Econ. Geol.* **104**, 635–668.

Large R. R., Halpin J. A., Danyushevsky L. V., Maslennikov V. V., Bull S. W., Long J. A., Gregory D. D., Lounejeva E., Lyons T. W., Sack P. J., McGoldrick P. J. and Calver C. R. (2014) Trace element content of sedimentary pyrite as a new proxy for deep-time ocean-atmosphere evolution. *Earth Planet. Sci. Lett.* **389**, 209–220.

Large R. R., Mukherjee I., Gregory D. D., Steadman J. A., Maslennikov V. V. and Meffre S. (2017) Ocean and atmosphere geochemical proxies derived from trace elements in marine pyrite: Implications for ore genesis in sedimentary basins. *Econ. Geol.* **112**, 423–450.

Large R., Thomas H., Craw D., Henne A. and Henderson S. (2012) Diagenetic pyrite as a source for metals in orogenic gold deposits, Otago Schist, New Zealand. *New Zeal. J. Geol. Geophys.* **55**, 137–149.

Li Y. H. and Schoonmaker J. E. (2013) *Chemical Composition and Mineralogy of Marine Sediments*.,

Little S. H., Vance D., McManus J. and Severmann S. (2016) Key role of continental margin sediments in the oceanic mass balance of Zn and Zn isotopes. *Geology* **44**, 207–210.

Little S. H., Vance D., Walker-Brown C. and Landing W. M. (2014) The oceanic mass balance of copper and zinc isotopes, investigated by analysis of their inputs, and outputs to ferromanganese oxide sediments. *Geochim. Cosmochim. Acta* **125**, 673–693.

Love L. G. (1971) Early diagenetic polyframboidal pyrite, primary and redeposited, from the Wenlockian Denbigh Grit Group, Conway, North Wales, U.K. *J. Sediment. Res.* **41**, 1038–1044.

Love L. G. (1957) Mircro-organisms and the presence of syngenetic pyrite. *Q. J. Geol. Soc.* **113**, 429–440.

Lowers H. A., Breit G. N., Foster A. L., Whitney J., Yount J., Uddin M. N. and Muneem A. A. (2007) Arsenic incorporation into authigenic pyrite, Bengal Basin sediment, Bangladesh. *Geochim. Cosmochim. Acta* **71**, 2699–2717.

Machel H. G. (2001) Bacterial and thermochemical sulfate reduction in diagenetic settings - old and new insights. *Sediment. Geol.* **140**, 143–175.

MacKinnon T. (1983) Origin of the Torlesse terrane and coeval rocks, South Island, New Zealand. *Geol. Soc. Am. Bull.* **94**, 967–985.

MacLean L. C. W., Pray T. J., Onstott T. C., Brodie E. L., Hazen T. C. and Southam G. (2007) Mineralogical, Chemical and Biological Characterization of an Anaerobic Biofilm Collected from a Borehole in a Deep Gold Mine in South Africa. *Geomicrobiol. J.* **24**, 491–504.

MacLean L. C. W., Tyliszczak T., Gilbert P. U. P. A., Zhou D., Pray T. J., Onstott T. C. and Southam G. (2008) A high-resolution chemical and structural study of framboidal pyrite formed within a low-temperature bacterial biofilm. *Geobiology* **6**, 471–480.

Moreau J. W., Webb R. I. and Banfield J. F. (2004) Ultrastructure, aggregation-state, and

crystal growth of biogenic nanocrystalline sphalerite and wurtzite. *Am. J. Sci.* **89**, 950–960.

Morse J. W. and Arakaki T. (1993) Adsorption and coprecipitation of divalent metals with mackinawite (FeS). *Geochim. Cosmochim. Acta* **57**, 3635–3640.

Morse J. W. and Luther G. W. (1999) Chemical influence on trace metalsulphide interactions in anoxic sediments. *Geochim. Cosmochim. Acta* **63**, 3378.

Mortimer N. (1993) Jurassic tectonic history of the Otago Schist, New Zealand. *Tectonics* **12**, 237–244.

Mortimer N. (2000) Metamorphic discontinuities in orogenic belts: example of the garnet-biotite-albite zone in the Otago Schist, New Zealand. *Int. J. Earth Sci.* **89**, 295–306.

Ohfuji H., Boyle A. P., Prior D. J. and Rickard D. (2005) Structure of framboidal pyrite: An electron backscatter diffraction study. *Am. Mineral.* **90**, 1693–1704.

Ohfuji H. and Rickard D. (2005) Experimental syntheses of framboids - A review. *Earth-Science Rev.* **71**, 147–170.

Picard A., Gartman A., Clarke D. R. and Girguis P. R. (2018) Sulfate-reducing bacteria influence the nucleation and growth of mackinawite and greigite. *Geochim. Cosmochim. Acta* **220**, 367–384.

Picard A., Gartman A. and Girguis P. R. (2016) What Do We Really Know about the Role of Microorganisms in Iron Sulfide Mineral Formation? *Front. Earth Sci.* **4**.

Pitcairn I. K., Teagle D. A. H., Craw D., Olivo G. R., Kerrich R. and Brewer T. S. (2006) Sources of metals and fluids in orogenic gold deposits: insoghts from the Otago and Alpone schists, New Zealand. *Econ. Geol.* **101**, 1525–1546.

Rickard D. (2012) *Sulfidic Sediments and Sedimentary Rocks*.

Rickard D. T. (1970) The origin of framboids. *Lithos* **3**, 269–293.

Sawlowicz Z. (1993) Pyrite framboids and their development: a new conceptual mechanism.

Geol. Rundschau **82**, 148–156.

Schoonen M. A. (2004) Mechanisms of sedimentary pyrite formation. *Spec. Pap. Soc. Am.* **379**, 117–134.

Tribovillard N., Algeo T. J., Lyons T. and Riboulleau A. (2006) Trace metals as paleoredox and paleoproductivity proxies: An update. *Chem. Geol.* **232**, 12–32.

Wacey D., Gleeson D. and Kilburn M. R. (2010) Microbialite taphonomy and biogenicity: New insights from NanoSIMS. *Geobiology* **8**, 403–416.

Wacey D., Kilburn M. R., Saunders M., Cliff J. B., Kong C., Liu A. G., Matthews J. J. and Brasier M. D. (2015) Uncovering framboidal pyrite biogenicity using nano-scale CNorg mapping. *Geology* **43**, 27–30.

Wilkin R. T. and Barnes H. L. (1997) Formation processes of framboidal pyrite. *Geochim. Cosmochim. Acta* **61**, 323–339.

Wilkin R. T., Barnes H. L. and Brantley S. L. (1996) The size distribution of framboidal pyrite in modern sediments: An indicator of redox conditions. *Geochim. Cosmochim. Acta* **60**, 3897–3912.

Xu J., Murayama M., Roco C. M., Veeramani H., Michel F. M., Rimstidt J. D., Winkler C. and Hochella M. F. (2016) Highly-defective nanocrystals of ZnS formed via dissimilatory bacterial sulfate reduction: A comparative study with their abiogenic analogues. *Geochim. Cosmochim. Acta* **180**, 274–275.

Yoon S. joung, Yáñez C., Bruns M. A., Martínez-Villegas N. and Martínez C. E. (2012) Natural zinc enrichment in peatlands: Biogeochemistry of ZnS formation. *Geochim. Cosmochim. Acta* **84**, 165–176.

Zhao Y., Vance D., Abouchami W. and de Baar H. J. W. (2014) Biogeochemical cycling of zinc and its isotopes in the Southern Ocean. *Geochim. Cosmochim. Acta* **125**, 653–672.

Zhou C., Vannela R., Hayes K. F. and Rittmann B. E. (2014) Effect of growth conditions on

microbial activity and iron-sulfide production by Desulfovibrio vulgaris. *J. Hazard. Mater.* **272**, 28–35.

Figure captions

Fig. 1 Geological map of the Otago Schist modified from Hu et al. (2015). The red rectangle on map is the sampling location.

Fig. 2 SEM observations of polyframboids and the corresponding EDS elemental maps of Zn and Fe. (a, b) Polyframboids consisting of framboids with zinc sulfide-rich and zinc sulfide-poor framboids; more detailed observation of framboids from box 1 and 2 are shown in Fig. 3; (c, d) Polyframboids with mixed framboids; (e, f) Pyrite-dominated framboids with few zinc sulfide microcrystals. NanoSIMS mapping areas were highlighted in yellow boxes.

Fig. 3 Detailed SEM observations of: (a) mixed framboids; and (b) pyrite-dominated framboids from boxes 1 and 2 in Fig. 2.

Fig. 4 The distributions of Fe (as $^{56}Fe^{32}S$) and Zn (as $^{65}Zn^{32}S$) on microcrystals. Linear element profiles were taken from x to x' (from the center to the boundaries of grains). Element counts were normalized to secondary electron (SE) counts. (a) Pyrite microcrystals with almost homogeneous Zn (type 1). On the profile, both Fe and Zn contents show similar trends. Normalized Zn counts are positively correlated with those of Fe. (b) Pyrite microcrystals with Zn concentrated on the boundaries (circled with dashed lines) (type 2). On the profile, Zn has relatively low counts in the centre of the grain, but high counts on the boundary where Fe content is relatively low. The spike occurring at around 1500 nm prior to

the increase of Zn counts is due to noise. Dashed lines on the profiles are used to indicate the boundaries of grains.

Fig. 5 (a) The distributions of Fe (as $^{56}Fe^{32}S$) and Zn (as $^{65}Zn^{32}S$) in a single framboid depicted in Fig. 2c. (b) Enlarged image of part of (a). The microcrystal circled with the dotted line has a core of pyrite and a rim of zinc sulfide (type 3), and that with a dashed line is zinc sulfide (type 4). (c) Normalized counts of Fe and Zn are plotted against each other with zinc sulfide (ZnS) and pyrite (FeS) analyses plotting in distinctly different areas.

Fig. 6 Distributions of CN (as $^{12}C^{14}N$) and Fe (as $^{56}Fe^{32}S$) in (a) pyrite microcrystals (in blue), and (b) pyrite (in blue) and zinc sulfide microcrystals (in green). Part (b) also shows the Zn (as $^{65}Zn^{32}S$) distribution. For a pyrite grain (type 2) in (a) and a zinc sulfide grain (type 4) in (b), linear profiles were taken from x to x' across the grains. The counts of elements (FeS, ZnS, CN and C_2) were extracted and normalized to secondary electron (SE) counts, shown on the corresponding graphs. CN index is also shown. Dashed lines on the profiles are used to indicate the boundaries of grains in (a) and (b) and "hole" area in (b).

Fig. 7 A general model of Zn sequestration processes in framboids, as an example of a single microcrystal. The detailed process has been discussed in the text. (Py: pyrite; BSR: bacterial sulfate reduction.)